EXPLORING THE NEGATIVE-TRIANGULARITY PATHWAY TO FUSION WITH MANTA

A.O. NELSON*, D. ARNOLD, W. BOYES, R. CHANDRA, H. CHOUDHURY, N. DASILVA, C. HANSEN, Y. LIU, P. LUNIA, C. PAZ-SOLDAN, M. PHARR, M. TOBIN, and H.S. WILSON
Columbia University
New York, USA
*Email: a.o.nelson@columbia.edu

J. L. BALL, R. BIELAJEW, S. BENJAMIN, M. CALVO-CARRERA, C. CHANG, L. CORSARO, C. CUMMINGS, A. DEVITRE, R. DIAB, S. FERRY, S. FRANK, J. JERKINS, J. JOHNSON, S. MACKIE, N. MANDELL, A. MARIS, M.A. MILLER, T. MOURATIDIS, D. MURPHY, E. PETERSON, P. RODRIGUEZ-FERNANDEZ, G. RUTHERFORD, A. SALTZMAN, S. SEGANTIN, J. VAN DE LINDT, A. VELBERG, A. WANG, M. WIGRAM, J. WITHAM, D. WHYTE
Massachusetts Institute of Technology
Cambridge, USA

Abstract

Many of the most pressing issues facing fusion reactors can be solved by adopting a tokamak design centered on the negative triangularity (NT) concept. The paper presents a fully-integrated reactor design, referred to as MANTA (Modular Adjustable Negative-Triangularity ARC), that exploits the NT shape to achieve $Q_{\text{electric}} > 1$, net electricity production greater than 50 MWe (peak) for three hours, a tritium breeding ratio greater than unity and an overnight cost of 3 billion US dollars. MANTA features a pulsed plasma capable of producing variable fusion power up to 500 MW without triggering edge localized modes. By exploiting natural advantages associated with the NT plasma shape, including outboard strikeline localization and robust particle transport, a divertor configuration capable of full integration with the nominal core scenario is designed. To enable rapid maintenance cycles and exploration of various reactor designs, a novel jointed toroidal field set is developed using REBCO superconductors. This configuration allows for plasma pulse lengths of up to 45 min with less than two minutes between pulses. Finally, a liquid immersion FLiBe blanket with positive tritium production is selected for heat management, consistent with an expected magnet lifetime of 1000 MW-years. In addition to the nominal MANTA design point, overarching guidance for NT reactor design is discussed, demonstrating significant promise for additional exploration and optimization of the NT reactor concept.

1. INTRODUCTION

Physically viable and economically attractive fusion pilot plants (FPPs) must be available by the 2030s to assist in reaching decarbonization targets. While significant progress has been made towards a viable tokamak reactor, many FPP designs employ plasma scenarios with significant implementation risks that could jeopardize the initial operation of such a device. In this report, we detail the design of an FPP based on the negative triangularity (NT) concept that utilizes the latest advances in fusion energy research to alleviate common risks associated with power handling in a reactor without compromising fusion performance. This design proposes a fundamental revision to the tokamak concept that should be seriously considered for reactor deployment.

The power handling problem is a fundamental hurdle for fusion reactors that stems from the need to contain fusion plasmas with tremendous temperatures on the order of 10s of keV. In the traditional H-mode tokamak, the stationary heat flux incident on plasma-facing components (PFCs), which is already enough to cause significant wear on machine components [1], is punctuated by energetic bursts from edge localized modes (ELMs) that are predicted to be strong enough to cause immediate melting and erosion [2]. This reality necessitates ELM mitigation and dissipative divertor solutions, which are often difficult to achieve simultaneously while maintaining fusion-relevant core conditions [3]. However, the adoption of a tokamak geometry with negative triangularity ($\delta < \delta_{\text{crit}} < 0$), where δ is defined as the average of the upper and lower triangularities $\delta_{\text{u},\ell} \equiv (R_{\text{geo}} - R_{\text{u},\ell})/a_{\text{minor}}$, offers key power handling advantages that have the potential to revolutionize the tokamak approach. (Here R_{geo} is the geometric major radius, $R_{\text{u},\ell}$ are respectively the major radius of the highest and lowest points along the plasma separatrix, and a_{minor} is the minor radius of the plasma.) The critical triangularity δ_{crit} is defined as the triangularity needed to close access to the 2^{nd} stability region for infinite-n ballooning modes (typically $0.15 < \delta_{\text{crit}} < -0.2$), as described in reference [4].

By destabilizing infinite-n ballooning modes in the plasma edge, NT plasmas obtain an inherent ELM-free state that is robust to broad changes in the plasma parameters, eliminating the risk that ELMs pose to PFCs in a reactor environment [4–6]. This ELM-free state is also characterized by suppression of the H-mode transition, enabling NT devices to operate at relatively low scrape-off-layer power P_{SOL}, which in turn allows NT operation both at high densities (Greenwald fractions $f_{\mathrm{GW}} \gtrsim 0.8$) and at high core radiation fractions ($f_{\mathrm{rad,core}} \gtrsim 0.7$) that may significantly reduce the steady-state power entering the divertor region [7–9]. Further, since the x-points in a NT geometry are farther from the magnetic axis, there is naturally more room in a NT reactor to implement large dissipative divertor regions [10–12]. Importantly, these characteristics of NT have been experimentally demonstrated to be compatible with high normalized performance (eg. $H_{98y2} \gtrsim 1$ and $\beta_{\mathrm{N}} \gtrsim 2.5$) [13]. This makes the NT geometry well suited to solving the power handling problem in tokamaks while maintaining sufficient core performance for electricity generation.

This paper documents the first integrated design for a negative triangularity tokamak, following the ARC compact-tokamak high-field approach [14–16]. Section 2 covers details relating to the high performance core scenario, as validated through turbulence modeling. Enabled by the ELM-free edge, compatibility with a dissipative divertor solution is discussed in section 3. Basic engineering considerations related to the magnet construction and handling of neutrons is discussed in section 4, showing that this machine can be reasonably constructed with existing technologies. The economic considerations of plant operation are discussed in section 5 before a brief concluding discussion in section 6.

2. CORE SCENARIO

The core plasma scenario employed in MANTA (Modular Adjustable Negative-Triangularity ARC) was obtained through a combination fast POPCON (Plasma OPerational CONtours) analysis [17] and higher-fidelity transport modeling with TGLF [18], informed where possible by NT experimental results [3–13, 19]. Initial scoping with POPCON modeling, which preforms power-balance calculations over a range of temperatures and densities, enabled rapid iterations of the nominal operating point as a self-consistent device model was constructed. During this process, the plasma shape (triangularity, elongation, major radius and aspect ratio) was scanned to obtain a rough solution that satisfied both the desired plasma performance (fusion power $P_{\mathrm{fus}} > 400\,\mathrm{MW}$ with heating power $P_{\mathrm{aux}} < 40\,\mathrm{MW}$) and the plant considerations (electrical gain factor $Q_{\mathrm{electrical}} > 1$ and net electric output $\geq 50\,\mathrm{MW_E}$ for at least 3 hours). The resulting equilibrium is shown in Fig. 1, which has a major radius of $R = 4.55\,\mathrm{m}$, a minor radius of $a = 1.2\,\mathrm{m}$, an average triangularity of $\delta = -0.47$ and an elongation of $\kappa = 1.4$. The final operating point also has a plasma current of $I_{\mathrm{p}} = 10\,\mathrm{MA}$ and an on-axis magnetic field of $B_0 = 11\,\mathrm{T}$, which leads to an edge safety factor of $q_{95} = 2.62$, consistent with other ARC-class devices [14–16]. To construct this equilibrium, a set of coils was designed using the FreeGS free-boundary Grad-Shafranov solver. The machine configuration is discussed in more depth in section 4. MANTA uses at 50-50 deuterium-tritium mixture for optimal fusion gain.

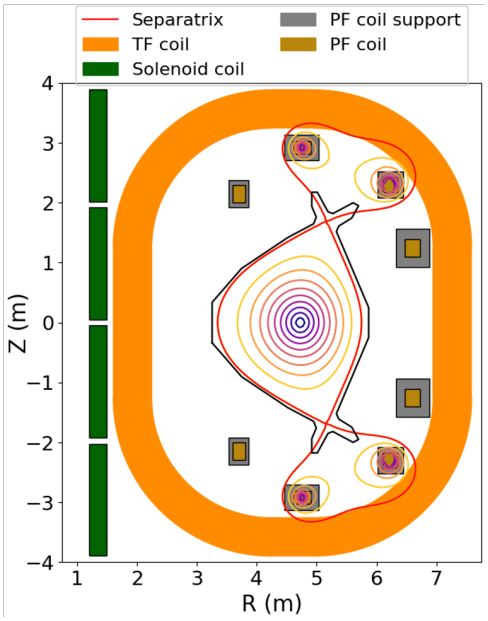

FIG. 1: *Poloidal cross-section of MANTA, including the solenoid, toroidal field (TF) and poloidal field (PF) coils. Space between the limiter and coils is reserved for the blanket.*

To obtain a more realistic core scenario, the nominal operating point was further refined through assessment with the TGYRO/TGLF transport model, which solves for temperature gradients in the core region by satisfying turbulent transport calculations [18]. The results from the TGLF calculations, which were run using the SAT2 saturation rule with fixed density profiles, are shown in Fig. 2. Notably, the absence of an H-mode transition at this strong negative triangularity [4], allows for the inclusion of a 0.1% Kr impurity population which radiates a significant amount of power from the core region (Fig. 2-c) and enables the self-consistent divertor solution presented in section 3. Due to this radiation, the power crossing the separatrix in these simulations is only $P_{\mathrm{SOL}} \sim 25.9\,\mathrm{MW}$ (equivalent to only $\sim 25\%$ of the predicted power needed to access

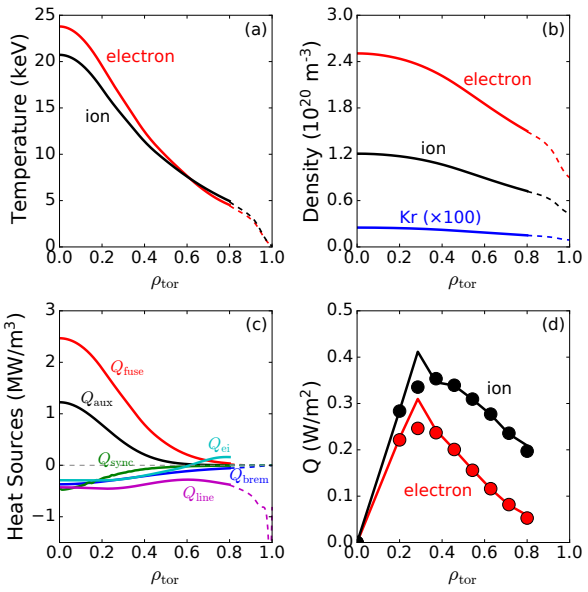

FIG. 2: *Profiles of (a) temperature and (b) density for the nominal MANTA operating scenario. (c) Heat sources included in the model. (d) The electron and ion heat transport (lines) are well converged with the model predictions (points).*

H-mode in a similar positive triangularity scenario [20]), despite producing fusion power of $P_{\text{fusion}} = 419.8\,\text{MW}$ with only $P_{\text{aux}} = 39.8\,\text{MW}$ of auxiliary heating power. Also shown in Fig. 2-c are the auxiliary heating profiles (Q_{aux}), the heat from fusion (Q_{fuse}), electron to ion heat transfer (Q_{ei}) and synchrotron (Q_{sync}) and Bremsstrahlung (Q_{brem}) radiation terms. Notably, the measures of the normalized performance obtained by this solution (normalized beta of $\beta_{\text{N}} = 1.1$, normalized confinement of $H_{98y2} = 0.81$ and Greenwald fractions of $f_{\text{GW}} = 0.79$) are all well within the operating spaces obtained by existing NT experiments on DIII-D and TCV [3, 7, 8, 13, 19], retiring a large portion of the physics risk typically associated with developing reactor scenarios. The heating scheme chosen for MANTA is lower hybrid radio frequency heating, which can deliver the necessary power at strong magnetic field and be tuned to deposit peak power on the $q = 2$ surface if needed to stabilize neoclassical tearing modes. The convergence of the TGLF simulations is shown in Fig. 2-d, showing good agreement between the model prediction (points) and output heat fluxes (lines) in the ion and electron channels. In addition to turbulence modeling, the infinite-n ballooning stability of this scenario was modeled with the BALOO code, confirming that the plasma is prevented from accidentally transitioning to an ELMing H-mode regime [4], suggesting that the core scenario presented here will be robustly ELM-free in addition to obtaining the performance targets outlined above. Notably, P_{fus} can be tuned directly by adjusting the equilibrium density. This offers a useful control knob in the form of variable gas fueling flow rate that could enable tailoring the fusion output of MANTA to meet the evolving power production needs over the course of the reactor lifetime. This sort of dynamic power control is much more difficult to perform in conventional tokamak reactors, which typically must sustain H-mode access to maintain high core performance.

3. DIVERTOR AND POWER HANDLING

A major benefit of NT is that the geometry inherently leads to a reduction in heat flux density on the divertor targets. NT moves the divertor to larger major radii, thereby increasing its surface area by order $\sim a^2$ compared to a positive triangularity plant of equivalent size. Furthermore, sufficiently negative triangularity ensures that the plasma remains in L-mode [4], avoiding the high heat fluxes caused by ELMs that an H-mode divertor must otherwise withstand and allowing for stationary operation at significant radiated power fractions. Despite these inherent advantages, as the plasma stored energy increases, proper power exhaust is essential to prevent significant component damage. As discussed above, a large component of the power in MANTA is radiated directly from the core plasma via impurity seeding. This power loads the vacuum vessel approximately uniformly and necessitates active cooling of the entire vacuum vessel surface. Heating of the vacuum vessel design (discussed in more depth in section 4) was modeled using fluid simulations in ANSYS Fluent [21]. Due to the efficient heat transfer between the cooling channel and blanket reservoir, all plasma-facing components survive the predicted heat flux from P_{rad} with a high margin of safety.

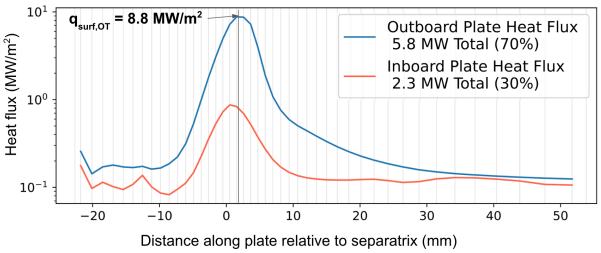

FIG. 3: *Total heat flux on the inner (orange) and outer (blue) divertor targets, as modeled by UEDGE. The peak heat flux remains under* $\sim 9\,MW/m^2$.

To calculate the heat and particle flux along the open fieldlines to the divertor target plates, the 2D edge transport code UEDGE was employed. UEDGE solves fluid equations for nearly-ionized, magnetized plas-

mas to determine their steady-state density and temperature. This is coupled to a fluid neutral solver to model the particle source and neutral dynamics in the simulation domain. UEDGE was used both to refine the point-design presented throughout this paper and to scope the parameter space surrounding the point-design, generally showing broad compatibility between predicted divertor conditions and material limits. Throughout this work, a fixed-fraction impurity model is used. The largest driving factor of the power handling performance is P_{SOL}, which was assumed to be $\sim$ 25 MW as predicted from the core modeling. A self-consistent separatrix density (n_{sep}) boundary condition at the core interface was also adapted from the core profiles. UEDGE then determines the electron and ion temperature at the separatrix, $T_{\mathrm{e,sep}}$ and $T_{\mathrm{i,sep}}$ respectively. From this edge solution, the heat flux incident on divertor targets for the nominal operating point is determined (see Fig. 3). No drifts are included in the simulation. The inner leg and inner SOL are found to be significantly colder than the outer components, leading to much greater heat loads on the outer target. However, the peak heatflux on the outer divertor remains below 9 MW/m^2, which respects the recrystallization temperature of tungsten (W) used as the target material. In the UEDGE model, close to full detachment of the inner target and partial detachment of the outer target was achieved, primarily through impurity seeding with neon. Enabled by the relatively low starting P_{SOL}, impurity scans demonstrate that an SOL neon impurity fraction of only $\sim 0.11\%$ is needed to achieve partially detachment in MANTA.

To understand the sensitivity of the point design to perturbations in divertor inputs, a 2D scan in operational space is performed. Given a particular fraction of impurity radiator, the robustness of divertor performance is tested against modifications to the assumptions for P_{SOL} or n_{sep}. To do this, the boundary conditions for power and density in UEDGE are varied independently, and the maximum heat flux on the divertor targets is calculated. For all combinations of P_{SOL} and n_{sep} the outer target remains the most thermally loaded, so it suffices to simply track the peak heat flux on the outer target ($q_{\mathrm{surf,OT}}$). Fig. 4 represents this quantity on the color bar of a scan of P_{SOL} ranging from $\sim 18 - 70$ MW and n_{sep} ranging from $0.6 - 1.3 10^{20}$ m^{-3}. Though there may be changes to the particle and heat transport as the power injected (and the fueling) changes, for simplicity, the transport coefficients are kept constant throughout this scan. Despite fixed transport, the density gradient clearly changes as the power is modified, potentially as a result of modifications in particle source. Regardless, it is clear that that there exists a wide range of the operational space in which $q_{\mathrm{surf,OT}} < 10$ MW/m^2, which is the assumed criteria for divertor survival [2]. Assuming $n_{\mathrm{sep}} = 10^{20}$ m^{-3} can be achieved, $P_{\mathrm{SOL}} = 35$ MW may still be acceptable, which is 10 MW higher than the nominal design point presented in section 2. For higher $n_{\mathrm{e,sep}}$, this margin grows even further. We note that figure 4 is created while assuming divertor regimes are not varying significantly. So, since MANTA's point design features attached outer legs and detached inner legs, these scans all remain in this regime. Presumably, increasing P_{net} for a given n_{sep} beyond that shown here will attach the inner legs and decreasing it will detach the outer legs. A more comprehensive discussion of this physics will be presented in future work.

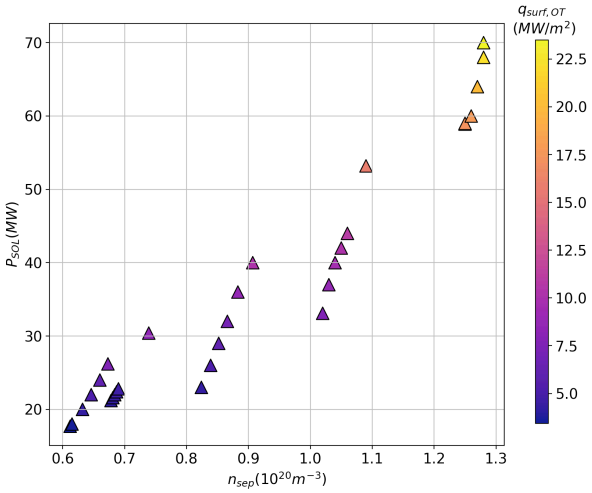

FIG. 4: *Divertor heat flux as a function of separatrix density and separatrix loss power. These scans, all with a SOL impurity content of $f_{\mathrm{SOL}} = 0.35\%$, show a broad range of acceptable operating conditions.*

4. ENGINEERING CONSIDERATIONS

The plasma scenario described above is enabled by access to the strong magnetic fields afforded by REBCO superconductors [22]. The design of the toroidal field (TF) magnets is driven by the need to provide high field on axis with REBCO tape while accommodating the shape of the liquid immersion blanket vessel, minimizing the length of superconductor needed, allowing demountable portions of the TF to enable easier maintenance [23], and keeping stress within engineering tolerances. To accommodate the unique NT plasma shape, several magnet designs were explicitly evaluated, including the traditional Princeton Dee [24], a reversed Dee, and a "window pane." Based on 2D-axisymmetric modeling of the stresses and strains in the coils, completed with the COMSOL multiphysics code [25], a variation of the window pane was chosen,

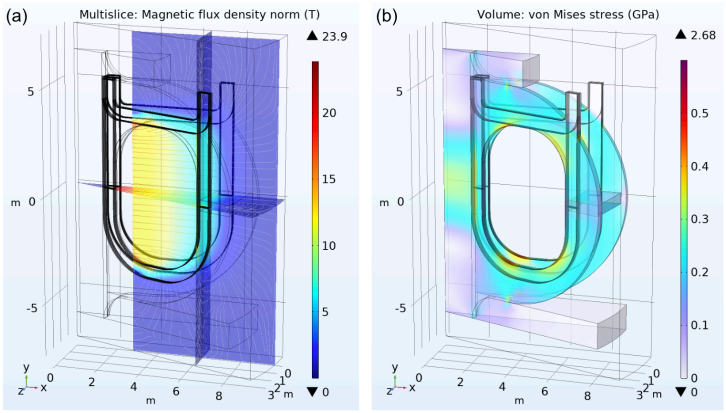

FIG. 5: *(a) Magnetic flux density and (b) von Mises stress for the "Viking horns" coil configuration chosen for MANTA.*

referred to here as the "Viking horns" design due to the horn-like protrusions at the top of the shape where the joints are located. This shape, depicted in Fig. 5, is able to achieve the required 11 T on-axis field with tolerable ($<$ 0.6 GPa) von Mises stress throughout the magnet volume and enables rapid maintenance of the internal poloidal field (PF) coils, blanket and vacuum vessel. Each TF is designed to operate at 47.2 kA with an inductance of 5.62 H and 288 turns split into 180 pancakes. As in the ARC design [14], we operate the REBCO at a sub-cooled temperature of 20K, far from its critical temperature, and employ a non-insulated coil for improved quench resilience. Design of the center stack and PF coils were completed individually, and will be described in depth in future work.

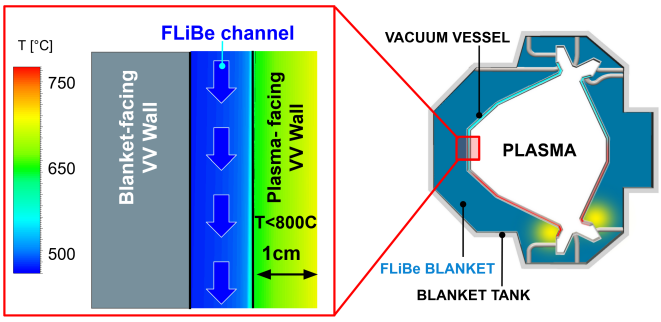

FIG. 6: *Schematic of the liquid FLiBe cooling channel and blanket.*

Since the MANTA plasma will produce significant quantities of high-energy neutrons as fusion products, a system to protect expensive, critical components from these damaging particles is an important consideration. It is vital that this neutronics system also be designed to most effectively harvest energy from and breed tritium using the neutrons to yield an efficient and self-sustaining reactor. This system, comprising the tritium breeding blanket as well as layers of dedicated neutron- and gamma ray-shielding material, was designed and optimized using the OpenMC Monte Carlo code [26]. In the final design, a toroidally continuous blanket tank surrounding the main vacuum vessel filled with flowing molten LiF-BeF_2 (FLiBe) enables a high tritium breeding ratio and improved reactor serviceability compared to other blanket designs [14]. The design also includes two 10 cm layers of shielding material around the blanket tank, with the inner layer made of tungsten carbide (WC) and the outer layer of boron carbide (B_4C). Outside these layers, in regions of higher neutron flux near the divertor, additional shields of 26 cm-thick B_4C provide extra protection. For compatibility with the expected heat and neutron loads, the vacuum vessel is planned to be a vanadium-chromium-titanium alloy (V-4Cr-4Ti). This material has been studied more than other candidates considered, and can be made compatible with the FLiBe blanket if MoF_6 is dissolved in the FLiBe, forming a protective barrier on the FLiBe-facing surface of the vessel [27, 28]. FLiBe channels in the first wall also provide active cooling to the plasma-facing tiles.

This blanket and shielding component design is further tuned to maximize the toroidal and poloidal field coil lifetimes, which are limited by a lifetime high energy (above 100 keV) neutron fluence of 3×10^{18} cm^{-2} [29, 30]. Though MANTA can have variable power output, neutron fluence scales linearly with the fusion power of the core, thus magnet lifetimes shown in Fig. 7 are in units of megawatt-years. The original target of 1,000 MWyr was achieved in the TF magnets even under the conservative assumption of a 100% duty cycle. This corresponds to a lifetime of about 2.5 years for the operating scenario described in section 2. The poloidal field coils, however, being closer to the plasma, experience higher neutron flux and must be replaced more frequently. This difference in magnet lifetimes inspired the demountable TF joints discussed above. These lifetimes and the flexible, modular design allow MANTA to meet its economic targets for a pilot plant.

5. ECONOMICS AND PLANT OPERATION

As done in previous ARC-class studies [14, 16], the total overnight plant cost and levelized cost of electricity (LCOE) are assessed for MANTA using a bottom-up costing estimation. The individual cost of each major tokamak system (heating, blanket, divertor, center stack, diagnostics, cryogenics, vacuum vessels, PF coils

and TF coils) as well as indirect costs, costs for balance of plant, site selection costs and other incidental costs (including financing, personnel, and capital degradation costs) are calculated individually. Three main methods are employed in estimating component costs, as appropriate for each: (1) extrapolating from current, experimental tokamaks and expert estimation, (2) costing raw materials and assuming a multiplication factor appropriate for the system complexity, and/or (3) referencing previous cost estimations for support systems, for example the ARPA-E report on fusion power plant costs [31]. This model predicts a plant total overnight cost for MANTA of roughly ∼$3 billion, less than the NASEM report target of less than $5 billion [32].

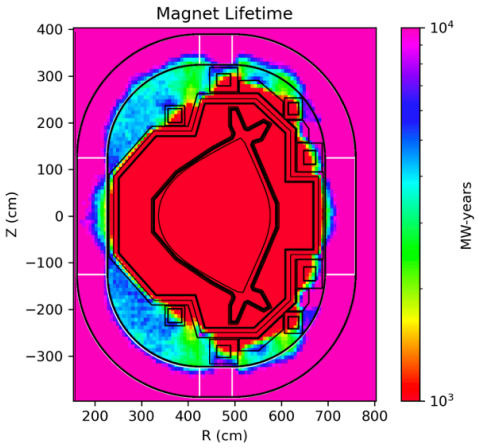

FIG. 7: *Calculated magnet lifetimes show that PF coils will require replacement over plant lifetime.*

The biggest driver of this cost comes from the TF magnets, which are predicted to cost around $1.3 billion. Since this represents over a third of the total plant cost, much of the uncertainty in the total cost estimation can also be credited to the TF systems, especially since an appropriate fabrication factor for this system is not yet well established. To gain more confidence in this costing estimation, the bottom-up approach is compared to the commonly applied updated Sheffield costing model, using equation A.6 from reference [33] and adjusting the coefficient of the term dependent on power removed to reflect net power production. The cost of the fusion island is the calculated according to equation A.7 in [33], and the volume of the fusion island according to equation 21 in [33]. With this implementation, an estimated overnight cost of ∼$3.3 billion is obtained, comparable to the bottom-up estimation and again safely less than the NASEM report limit [32]. Given the expected plant output, this total cost translates to a unit cost of ∼$25 million / MWe, comparable to an offshore win

A more complete economic case for any proposed FPP demands an accounting of the lifetime costs and revenue streams. Such accounting also enables a calculation of the LCOE, which is the minimum wholesale price of electricity at which the project becomes profitable. The LCOE for MANTA is calculated as:

$$LCOE = \frac{\sum_t C_t}{(1+d)^t} \Big/ \frac{\sum_T P_T}{(1+d)^t}, \qquad (1)$$

where C_t is the cost at a specific timepoint, P_t the electricity generated at that time and d is a discounting factor. Several assumptions are included in this calculation, including a 3% interest rate, 0% down-payment, 15$M/yr in personnel costs, and a 0.5% yearly capital degradation cost and that the entire loan for the capital cost (including plant, facilities, and decommissioning) is payed off by the end of the project. Further, fabrication and replacement of damaged systems, including one lifetime vacuum vessel replacement, and nearest half-year replacements of the REBCO portion of magnet systems are included alongside an effective electric duty cycle of 94% (as some portion of the thermal power is used to charge the thermal reservoir to maintain constant electricity producing during CS swings), a maintenance downtime of 6% and a turbine efficiency of 36%. After replacing the 900g startup tritium inventory, we define fueling as a negative cost due to selling tritium at an assumed current price of $30k/g. We apply an industry standard discounting rate of 7% and inflation rate of 3%. For a three year project, using $47.6/MWhr cost of electricity, we find that the total project cost remains at $3.0B, as shown in Fig. 8. Periods of zero electric production/consumption during magnet replacement are evident.

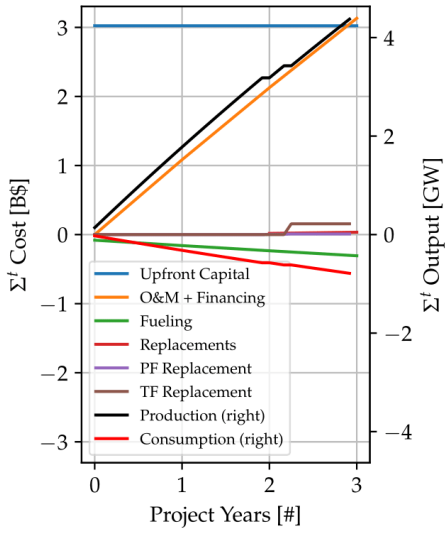

FIG. 8: *Cost and electricity estimations for a three year MANTA project.*

To meet the goal of 50MWe net electricity production for 3 hours, this study includes a preliminary thermal plant design. The FLiBe immersion blanket acts as the primary coolant loop, performing crucial fuel cycle and neutronics while also exchanging heat with a secondary solar salt (60 NaNO3 40 KNO3). The use of

a secondary loop reduces both the required volume of FLiBe as well as the number of systems exposed to radiation. This mixture of molten salts has a boiling point below the hot leg of the primary cycle and a freezing point above the cold leg of the power conversion cycle [34]. Both subcritical and supercritical Rankine cycles were found to be viable tertiary loop options for generating the plant's electricity. In order to maximize turbine efficiency, a thermal storage system is integrated into the secondary loop that provides constant thermal power to the Rankine cycle despite the pulsed core scenario.

The fuel cycle for MANTA was modeled using the Simulink toolbox in MATLAB [35]. This model accounts for (among other factors) tritium startup inventory, fuel burn fraction in the plasma, and tritium losses in the system. Due to the relatively high number of unknowns in this process, more conservative estimates for model parameters (e.g. tritium losses, system inefficiency, startup inventory, availability factor) are used. Two of the most sensitive parameters of the fuel cycle that require careful consideration are the startup and reserve tritium inventories. While the startup inventory can be simply calculated from the other variables, the reserve inventory (i.e. how much extra tritium is stored at the plant) necessitates a balance between radiation safety, cost, and the likelihood of a system failure. We adopt an extremely conservative estimate of a 75g reserve inventory, from which a required startup inventory of 440g is calculated. As tritium fuel systems further mature, these numbers will likely drop, relaxing both economic and safety concerns. As presented here, a tritium breeding ratio of 1.11 allows for excess tritium productionfor use to start up future plants.

6. DISCUSSION AND CONCLUSION

The preliminary MANTA design presented here offers a significant deviation from traditional tokamak reactors by exploiting inherent properties of negative triangularity scenarios to approach FPP design from a power-handling first perspective [11]. By adopting a plasma shape with $\delta < \delta_{\text{crit}} < 0$, ELMs are robustly suppressed without sacrificing the reactor-compatibility of the core plasma [4]. Operation at low P_{SOL}, high f_{GW} and high $f_{\text{rad,core}}$ are also enabled by NT operation. Together these properties allow for a self-consistent core and edge plasma solution that exceeds the performance targets proposed by the 2021 NASEM report [32] without requiring significant advances in materials or magnets technology. Additional efforts to refine, validate and optimize the MANTA design point will be presented in future work.

ACKNOWLEDGEMENTS

This work was predominately completed during a tokamak design course hosted jointed by the Massachusetts Institute of Technology and Columbia University. All authors listed contributed equally to this work.

REFERENCES

[1] EICH, T. & SIEGLIN, B. & SCARABOSIO, A. & FUNDAMENSKI, W. & GOLDSTON, R. J., and HERRMANN, A., Inter-ELM power decay length for JET and ASDEX Upgrade: Measurement and comparison with heuristic drift-based model, Phys. Rev. Lett. **107** (2011) 215001.

[2] GUNN, J. P. *et al.*, Surface heat loads on the ITER divertor vertical targets, Nucl. Fusion **57** (2017).

[3] PAZ-SOLDAN, C., Plasma performance and operational space without ELMs in DIII-D, Plasma Phys. Control. Fusion **63** (2021).

[4] NELSON, A. O. & PAZ-SOLDAN, C., and SAARELMA, S., Prospects for H-mode inhibition in negative triangularity tokamak reactor plasmas, Nucl. Fusion **62** (2022).

[5] MERLE, A. & SAUTER, O., and YU MEDVEDEV, S., Pedestal properties of H-modes with negative triangularity using the EPED-CH model, Plasma Phys. Control. Fusion **59** Publisher: Institute of Physics Publishing (2017).

[6] SAARELMA, S. *et al.*, Ballooning instability preventing the H-mode access in plasmas with negative triangularity shape on the DIII-D tokamak, Plasma Phys. Control. Fusion **63** (2021).

[7] CAMENEN, Y. *et al.*, Electron heat transport in shaped TCV L-mode plasmas, Plasma Phys. Control. Fusion **47** (2005) 1971–1987.

[8] MARINONI, A. *et al.*, Diverted negative triangularity plasmas on DIII-D: The benefit of high confinement without the liability of an edge pedestal, Nucl. Fusion **61** (2021).

[9] FAITSCH, M. *et al.*, Dependence of the L-Mode scrape-off layer power fall-off length on the upper triangularity in TCV, Plasma Phys. Control. Fusion **60** (2018) 045010.

[10] MEDVEDEV, S. Y. *et al.*, The negative triangularity tokamak: Stability limits and prospects as a fusion energy system, Nucl. Fusion **55** (2015).

[11] KIKUCHI, M. *et al.*, L-mode-edge negative triangularity tokamak reactor, Nucl. Fusion **59** (2019).

[12] NELSON, A. O. *et al.*, Vertical Control of DIII-D Discharges with Strong Negative Triangularity, Plasma Phys. Control. Fusion **65** (2023).

[13] AUSTIN, M. E. *et al.*, Achievement of Reactor-Relevant Performance in Negative Triangularity Shape in the DIII-D Tokamak, Phys. Rev. Lett. **122** (2019).

[14] SORBOM, B. N. *et al.*, ARC: A compact, high-field, fusion nuclear science facility and demonstration power plant with demountable magnets, Fusion Eng. Des. **100** (2015) 378–405.

[15] KUANG, A. Q. *et al.*, Conceptual design study for heat exhaust management in the ARC fusion pilot plant, Fusion Eng. Des. **137** Publisher: Elsevier Ltd (2018) 221–242.

[16] FRANK, S. *et al.*, Radiative pulsed L-mode operation in ARC-class reactors, Nucl. Fusion **62** (2022).

[17] HOULBERG, W. & ATTENBERGER, S., and HIVELY, L., Contour analysis of fusion reactor plasma performance, Nucl. Fusion **22** (1982) 935–945.

[18] STAEBLER, G. M. & KINSEY, J. E., and WALTZ, R. E., A theory-based transport model with comprehensive physics, Phys. Plasmas **14** (2007) 055909.

[19] POCHELON, A. *et al.*, Recent TCV results - Innovative plasma shaping to improve plasma properties and insight, Plasma and Fusion Research **7** (2012).

[20] MARTIN, Y. R. and TAKIZUKA, T., Power requirement for accessing the H-mode in ITER, Journal of Physics: Conference Series **123** (2008).

[21] ANSYS, INC., Ansys Fluids Software (2016).

[22] MCINTYRE, P. M. & ROGERS, J., and SATTAROV, A., Blocks-in-Conduit: REBCO Cable for a 20T@20K Toroid for Compact Fusion Tokamaks, IEEE Transactions on Applied Superconductivity **31** (2021) 1–5.

[23] MANGIAROTTI, F. J. & GOH, J. & TAKAYASU, M. & BROMBERG, L. & MINERVINI, J. V., and WHYTE, D., Demountable Toroidal Field Magnets for Use in a Compact Modular Fusion Reactor, Journal of Physics: Conference Series **507** (2014) 032030.

[24] THOME, R. J. and TARRH, J. M., MHD and fusion magnets: Field and force design concepts Publisher: John Wiley and Sons, Inc.,New York, NY (1982).

[25] COMSOL INC., COMSOL Multiphysics 4.3b (2013).

[26] ROMANO, P. K. & HORELIK, N. E. & HERMAN, B. R. & NELSON, A. G. & FORGET, B., and SMITH, K., OpenMC: A state-of-the-art Monte Carlo code for research and development, Annals of Nuclear Energy **82** (2015) 90–97.

[27] SZE, D.-K., IPFR, Integrated Pool Fusion Reactor Concept, Fusion Technology **10** (1986) 875–880.

[28] MUROGA, T., Vanadium Alloys for Fusion Blanket Applications, MATERIALS TRANSACTIONS **46** (2005) 405–411.

[29] FISCHER, D. X. & PROKOPEC, R. & EMHOFER, J., and EISTERER, M., The effect of fast neutron irradiation on the superconducting properties of REBCO coated conductors with and without artificial pinning centers, Superconductor Science and Technology **31** (2018) 044006.

[30] PROKOPEC, R. & FISCHER, D. X. & WEBER, H. W., and EISTERER, M., Suitability of coated conductors for fusion magnets in view of their radiation response, Superconductor Science and Technology **28** (2015) 014005.

[31] WOODRUFF, S. & MILLER, R. & CHAN, D. & ROUTH, S. & SAKTI BASU, and RAO, S., Conceptual Cost Study for a Fusion Power Plant Based on Four Technologies from the DOE ARPA-E ALPHA Program Publisher: Unpublished (2017).

[32] NATIONAL ACADEMIES OF SCIENCES ENGINEERING AND MEDICINE, Bringing Fusion to the U.S. Grid. Washington, D.C.: National Academies Press, (2021).

[33] SHEFFIELD, J. and MILORA, S. L., Generic Magnetic Fusion Reactor Revisited, Fusion Sci. and Technol. **70** (2016) 14–35.

[34] SOHAL, M. S. & EBNER, M. A., and SABHAR, P., Engineering database of liquid salt thermophysical, Idaho National Lab.(INL), Idaho Falls, ID (United States) (2013).

[35] THE MATHWORKS INC., Simulink version: 10.4 (R2021b) (2022).